Numerical study of the human walking-induced fine particles resuspension

Amir Boulbair, Ahmed Benabed, Bart Janssens, Karim Limam, Walter Bosschaerts

Version of Record: https://www.sciencedirect.com/science/article/pii/S0360132322002906
Manuscript_8140d18a4d0f55e19709d286267f2656

Numerical study of the human walking-induced fine particles resuspension

Amir Boulbair[1,2], Ahmed Benabed[3], Bart Janssens[2], Karim Limam[1], Walter Bosschaerts[2]

[1]LaSIE, University of La Rochelle, Av. M. Crépeau, 17042 La Rochelle Cedex 01, France
[2]Royal Military Academy, Rue Hobbema 8, Brussels, Belgium
[3]Departement of Mechanical and Environmental Engineering, ESTACA, Paris-Saclay Campus, 78180, Montigny-le-Bretonneux, France.

Abstract

One of the main sources of pollution in indoor environments is human walking-induced particle resuspension. In this work, the airflow and resuspension of particles smaller than 1 µm generated by foot tapping were investigated numerically using ANSYS CFX software. The k-ω shear stress transport model was considered to simulate the unsteady airflow field around and under the shoe. The immersed solid method was then used to incorporate the shoe in a three-dimensional computational domain. Particle resuspension was predicted by means of the Rock 'n' Roll model. The effects of the walking speed and shoe groove pattern (transverse grooves, longitudinal grooves and no groove) were studied. Three different selected particle-substrate combinations (ATD-linoleum, PSL-linoleum and alumina-steel) were tested. The numerical simulations showed that the air below the foot was ejected as a high velocity jet. After the shoe hit the ground, counterrotating vortices were formed around the shoe. The results of particle resuspension were compared with previous experimental works, and good agreement was found. Results shown that for the different studied cases the resuspension fraction ranges over four orders of magnitude, from 10^{-5} to 10^{-1}. Particle resuspension fractions increased with particle size and walking speed. However, no significant influence of the shoe groove patterns was observed.

Keywords: Indoor air quality; Particle resuspension; Shoe groove pattern; Induced airflow; Walking speed; Particle-substrate combination.

1. Introduction

People spend most of their time indoors, which leads to important exposure to contaminating elements from different types of particles. Epidemiological and toxicological studies have shown that many health effects are caused by particulate matter (PM) [1], which is defined as a complex mixture of microscopic solid or liquid matter suspended in the air. Particles are classified according to their aerodynamic diameter as fine particles (PM10, PM2.5, and PM1) or ultrafine particles (PM0.1). Ref. [2] revealed that most of the particle mass (82%) is attributable to particles sized from 0.1 to 0.5 µm. One of the main sources of PM pollution in indoor environments is human walking-induced particle resuspension [3, 4, 5].

To better understand particle resuspension, several experimental studies have been conducted. These works investigated the influence of many parameters on this phenomenon, including flooring properties (Hardness [6, 7], roughness [8]), surface dust loading [5, 9], environmental factors (relative humidity) [10, 11, 5] and human-related factors, such as shoe type [12, 13], walking speed [14, 15, 5], and particle properties (Origin, density …) [5, 16]. Most of these works showed that human walking in indoor environments contributes significantly to increase fine particle concentration. Recently, Ref. [7] showed that human walking can resuspend particles with sizes ranging from 0.01 to 0.1 µm.

Studying physical phenomena by numerical simulation has become very attractive and cost-effective, especially with the increase in computer performance. This approach allows the investigation of several phenomena, related to fluid mechanics, and offers researchers better control over the influencing parameters and especially more accurate results. However, only a few studies on particle resuspension have been carried out numerically. This is due to the complexity of the human walk [6] and the difficulty to introduce the step into the computational domain. To overcome this difficulty, some authors have used analytical solutions or numerical simulations with some simplifying assumptions. Table 1 lists the four key numerical studies on human walking-induced particle resuspension, their resuspension model, and some inlet parameters. Ref. [12] studied resuspension, deposition, and spreading of particles from floors due to human walking. The authors modeled the stepping motions of the foot, down and up, using a combination of two circular disks (one for the toe and one for the heel). They developed a model for particle detachment and resuspension based on particle-wall adhesion force and the hydrodynamic drag and lift forces. The authors supposed that airflow was laminar in the region between de the shoe and the floor. Their results show that shallower grooves, higher surface roughness, larger shoe size, and

higher walking speed (up and down) increase the concentrations of resuspended particles. Ref. [17] investigate the effect of walking forward, stamping in place, and stamping in place while rotating of a human on particle resuspension. The authors modeled the resuspension of 2.7 µm and 7.7 µm particles using a classical adhesive force model. They reveal that the resuspended mass in the case of human motion with rotation is two times greater than that of the case without rotation. Also, the magnitude of the adhesive force has little effect on the modeled resuspension event. Ref. [18] investigated particle resuspension from the carpet layer during a footstep using a large eddy simulation and immersed boundary method. To model particle detachment from the floor, they implemented the energy accumulation model Rock 'n' Roll [19, 20, 21]. This model assumes that a particle is resuspended when it has accumulated enough vibrational energy from the turbulent flow to detach itself from the surface. The authors performed their simulation with three constant speeds and three particle sizes (5 µm, 10 µm, and 20 µm). They observed that their simulations underestimate the resuspension rate, with an order of magnitude difference compared to the experiments. Ref. [22] investigated particle resuspension due to footstep using an unsteady Reynolds Averaged Navier-Stokes equations (URANS) approach coupled with the RNG K-epsilon turbulence model. They employed the Monte Carlo simulation model of Ref. [16, 23]. This is relevant for modeling the particle resuspension induced by the shoe. It is based on the balance of forces applied to a spherical particle with a number of bumps on them to model irregularly shaped particles. The authors used two different particle sizes of 5-7.5 µm and 7.5-10 µm. The simulation results showed a high number of resuspended particles in the size range of 5-7.5 µm compared to 7.5-10 µm.

Table 1: Four key numerical studies on human walking-induced particle resuspension.

Ref	Particle sizes (µm)	Foot speed	Particle-surface combination	Particle resuspension model
[12]	1, 2, 3, 4, 5, 7, 10, 20	The step-down velocity of the toe: $V_f = 0.5$ m/s. The step-down velocity of the heel: $V_f = 0.1$ m/s. The initial step up velocity of the toe: $V_f = 0.065$ m/s. The initial step up velocity of the heel: $V_f = 0.033$ m/s.	•Silicon dioxide- silicon dioxide •Aluminum oxide-aluminum oxide •Vinyl tile-vinyl tile •Silicon dioxide-vinyl tile •Aluminum oxide-vinyl tile	Rolling detachment of particle (particle is considered as detached when the external force moment overcomes the resisting moment due to the adhesion force).
[17]	2.7, 7.7	Case 1: Human walking and stamping. Case 2: Human walking, stamping and rotating (the foot speed was not specified).	Carpet (adhesive force coefficient A_a range from 3.8×10^{-12} to 6×10^{-4} J·m/kg)	Force balance (drag and adhesion forces)
[18]	5, 10, 20	Constant angular velocity 21°/s, 28°/s, and 35 °/s.	The authors used carpet as a flooring material with surface energy corresponding to the Alumina-steel combination.	Rock 'n'Roll
[22]	5-7.5, 7.5-10	Constant angular velocity 0.5 step/s.	ATD-Vinyl	Monte Carlo simulation model

These works have shown the influence of foot speed and particle size on this phenomenon. However, no numerical study has quantified the resuspension of particles smaller than 1.0 µm. In addition, in the most of previous studies the step velocity was considered as a constant. Moreover, there are still differences for some parameters (shoe grooves), not only between the experimental works themselves, but also with the results of the numerical studies. The main goal of this work is to study the resuspension of particles of sizes ranging from 0.1 to 1 µm under different conditions. This study has required a thorough study of the flow created by the step using realistic step velocities as boundary conditions. The immersed solid method was used to incorporate the shoe in a three-dimensional geometry. The Rock 'n' Roll model suggested by Ref. [21] was considered to predict particle resuspension. Then, the particle resuspension fraction was applied to compare different cases. The effects of the particle-substrate combinations (ATD-linoleum, PSL-linoleum, and alumina-steel), walking speed and shoe groove pattern (transverse grooves, longitudinal grooves, and no groove) were also studied. The results of particle resuspension were then compared with previous experimental works, and a good agreement was found.

2. Numerical simulation

2.1 Numerical scheme

In this work, ANSYS CFX software was used to investigate the airflow and particle resuspension generated by human foot tapping during walking. The computational domain consists of a small-scale chamber with a floor area of 50 cm×40 cm and a height of 30 cm. A size 42 EU shoe (Figure 1) was made under Autodesk Inventor and embedded into the computational domain as an immersed object. This shoe was chosen based on the previous work of Ref. [7]. The initial angle between the shoe and the floor (24 °) and the angular velocity of the shoe were measured experimentally (see Section 2.2). The immersed solid method available in CFX was used to simulate the moving shoe. Figure 1 represents the geometry and the position of the shoe.

For our simulations, the fluid is initially at rest and at atmospheric pressure and assumed to be incompressible. The constant fluid properties are ν=15.1×10^{-6} kg.m^{-1}.s^{-1}, T=25 °C, and ρ=1.225 kg/m^3. A non-slip condition is then applied along the walls. The URANS simulation with the k-ω shear stress transport model was used to simulate the unsteady flow of the air in the computational domain. This model remains a good compromise between accuracy and calculation time [24].

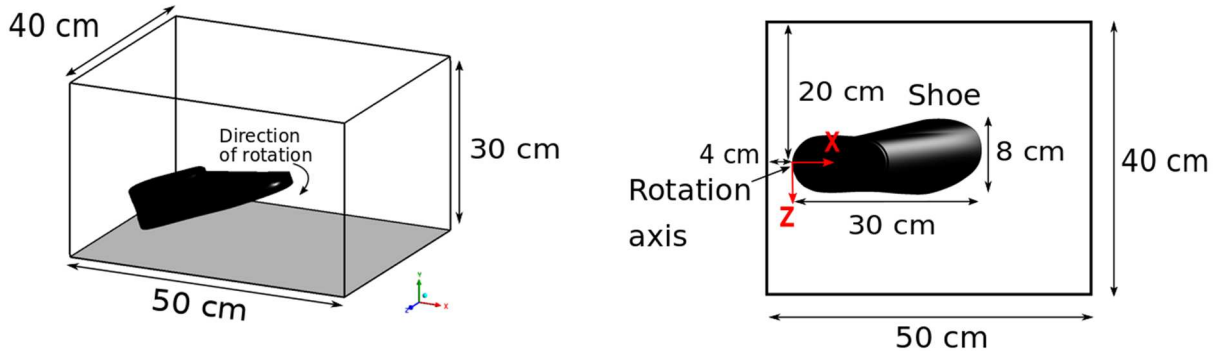

Figure 1. Geometry of the chamber and position of the shoe.

2.1.1 The immersed solid method

The immersed solid is a fluid-structure interaction method within ANSYS CFX that allows for the simulation of solid objects moving through fluid regions while avoiding deformation and remeshing [25]. This method is particularly useful in our case, as the volume of the mesh under the shoe is reduced to zero when the shoe touches the ground. The immerged solid domain occupies the same amount of space as a portion of the fluid domain containing the immerged solid. In this method, the influence of the immersed solid on the surrounding fluid is forced to move at the velocity of the solid by applying the source term in the fluid equations. Momentum sources for the immersed solid $\boldsymbol{S}$ are equal to Equation (1) [26]:

$$\boldsymbol{S} = -\alpha\beta C_M(\boldsymbol{U} - \boldsymbol{U^F}) \qquad (1)$$

where $\boldsymbol{U}$ is the fluid velocity vector (m/s), $\boldsymbol{U^F}$ is the forcing velocity due to the immersed solid (m/s), C_M is the momentum source coefficient (A large number evaluated as the average of the three diagonal coefficients in the momentum equation), α is the momentum force scaling factor which controls the size of the source term (set to the default value of 10), and β is the forcing function. If near-wall treatment is not activated near the immersed solid boundary, the β function is set to be zero for fluid nodes lying outside the immersed solid domain, and one for fluid nodes inside the immersed solid. If near-wall treatment is used, the β function is set to be volume-averaged inside function so that the β values and the corresponding forcing terms near the immersed boundary will be non-zero. The volume-averaged inside function averages the inside function, weighted by the nodal volume [26].

2.1.2 Resuspension fraction estimation

There are several parameters used to estimate human walking-induced resuspension, such as the resuspended fraction and the particle emission rate. To compare our numerical results with those of Ref. [7], the resuspension fractions were used to estimate the particle resuspension. This parameter can be calculated as the ratio between

the total resuspended mass m_R(kg) and the initial deposited particle mass in the resuspension area m_0(kg), as shown in Equation (2).

$$r_{rs,i} = \frac{m_R}{m_0} \qquad (2)$$

The total resuspended mass can be estimated as the integral of the resuspended particle mass flow rate from the ground (kg/s) over the time (see Equation (3)).

$$m_R = \int_0^{t_f} q_m(t)dt \qquad (3)$$

where t_f is the total simulated time (s) and $q_m(t)$ is the resuspended particle mass flow rate from the ground (kg/s).

Due to the volumetric nature of the particles, the numerical implementation of the particles in the computational domain requires the creation of a volume reservoir in the first grid cells on the ground. In this reservoir, the resuspended particles are modeled by a particle source from the different cells. The mass flow rate from the surface is equal to the sum of all integrals over the volumes of the ground cells of the particle source (see Equation (4)).

$$q_m(t) = \sum_{i=1}^{n} \int_{V_i} S_{p_i}(t)dV_i \qquad (4)$$

where V_i is the volume of the first cell (m^3) at location i, n number of first cells and S_{p_i} is the particle source generated in a given first cell (kg.m^{-3}.s^{-1}) which represents the amount of suspended particles from the first cell at each time step, it can be calculated using Equation (5) [27]:

$$S_p = \bar{\Lambda}(t)C_s\,(t) \qquad (5)$$

where $\bar{\Lambda}(t)$ the average resuspension rate (s^{-1}) given by Equation (23) (further details about $\bar{\Lambda}(t)$ are in section 2.1.3).

$C_s\,(t)$ is the particle surface loading at time t (in the first grid cell) (kg/m^3). The particle surface loading decreases over time, due the resuspension, was considered using the Equation (6).

$$C_s\,(t + \Delta t) = C_s(t)(1 - \bar{\Lambda}(t)\Delta t) \qquad (6)$$

where $C_s\,(t + \Delta t)$ is the concentration at time $t + \Delta t$ (kg/m^3).

In this work, an Eulerian-Eulerian approach was used to model particle concentration in the domain. In this approach, the particle concentration is taken into account using the scalar transport equation (see Equation (7)).

$$\frac{\partial C}{\partial t} + \nabla.(\boldsymbol{U}C) = \nabla.\left(\left(D + \frac{\mu_t}{\rho Sc_t}\right)\boldsymbol{\nabla} C\right) + S_p \qquad (7)$$

where C is the particle concentration (kg/m^3), ρ is the fluid density (kg/m^3), $\boldsymbol{U}$ is the fluid velocity vector (m/s), μ_t is the eddy viscosity (Pa.s), Sc_t is the turbulent Schmidt number, and D is the particle diffusion coefficient (m^2/s) in this study was taken 10^{-5} m^2/s [26].

In this work, the initial deposited particle mass in the resuspension area can be calculated using Equation (8).

$$m_0 = C_0 V_t = C_0 H_{fc} A_s \qquad (8)$$

C_0 is the initial floor loading (kg/m^3), and V_t (m^3), A_s (m^2) and H_{fc} (m) represent the volume, the height and the area of the cell from which particles are resuspended after the foot-step. The resuspension area depends on many parameters, such as the walking style, the footstep intensity, and the surface characteristics of the shoe sole. However, this surface is not easy to determine; thus, in this work, we set it equal to the contact area of the shoe sole.

The initial floor loading values considered in this work are represented in Figure 2. These concentrations were calculated based on the surface loading (particles/m^2) from the work of Ref. [7] by assuming that the particles were spherical and that the same mass was deposited in the floor.

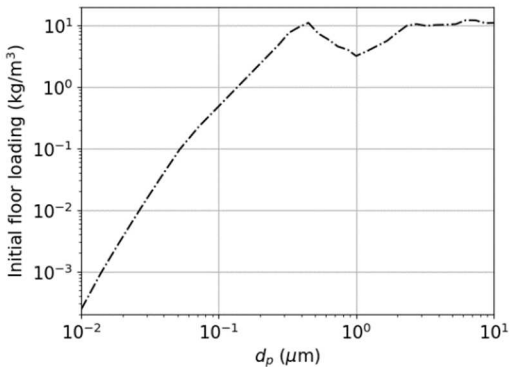

Figure 2. Initial floor loading.

2.1.3 Particle resuspension model

In this study, particle resuspension was estimated based on the Rock 'n' Roll model developed by Ref. [21]. Based on the accumulation of energy, particles of diameter d_p are assumed to be deposited between two-point asperity contacts (P and Q) of a rough surface (Figure 3). This particle resuspends by the effect of the turbulent airflow following the mechanism shown in Figure 3. The particle will rock about point P due to the action of the aerodynamic lift (F_L) and drag (F_D) forces, as they are counteracted by the adhesive force f_a at point Q until it has sufficient rotational energy to break the contact at point Q [20]. After this, the particle rotates or lifts off.

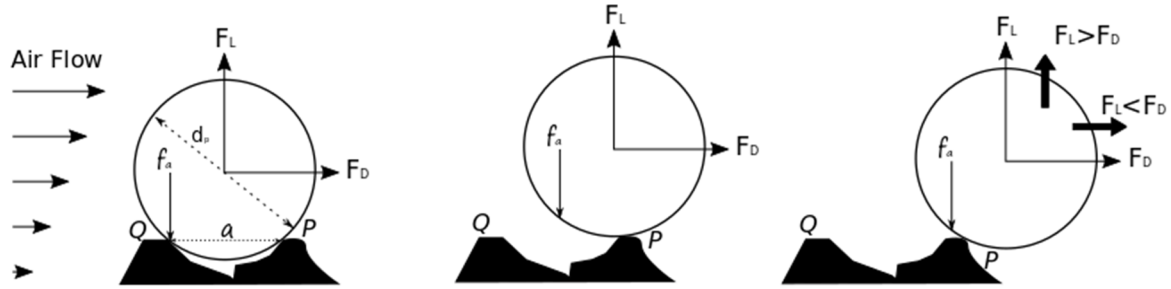

Figure 3. Scheme of the movement of a particle placed on a rough surface between two asperities P and Q and exposed to an air flow according to the Rock 'n' Roll model [21].

The resuspension rate $\Lambda(t)$ (1/s) can be estimated using Equation (9) [21]:

$$\Lambda(t) = \int_0^\infty \varphi(\overline{f_a}) p(\overline{f_a}) e^{-p(\overline{f_a})t} d\overline{f_a} \qquad (9)$$

where $\overline{f_a}$ is the normalized adhesive force, p is the resuspension rate constant and $\varphi(\overline{f_a})$ is the distribution of normalized adhesive forces.

The normalized adhesive force is the ratio of the adhesive force for a real rough substrate f_a (N) to the adhesive force F_a (N) for a perfectly smooth substrate.

$$\overline{f_a} = \frac{f_a}{F_a} \qquad (10)$$

For a sphere of radius r (m), the adhesive force for a smooth substrate is given by:

$$F_a = \frac{3}{2}\pi W_a r \qquad (11)$$

where W_a (J/m^2) is the thermodynamic work of adhesion between the particles and the substrate.

In this model, the distribution of normalized adhesive forces is assumed to be a lognormal as shown by Equation (12).

$$\varphi(\overline{f_a}) = \frac{1}{\sqrt{2\pi}}\left(\frac{1}{\overline{f_a} ln(\sigma_a')}\right) \exp\left(-\frac{1}{2}\left\{\frac{ln\left(\frac{\overline{f_a}}{\langle \overline{f_a} \rangle}\right)}{ln(\sigma_a')}\right\}^2\right) \quad (12)$$

where $\langle \overline{f_a} \rangle$ is the geometric mean of the normalized adhesive forces and σ_a' is the geometric standard deviation of the adhesive forces. These two parameters can be estimated for particles diameters ranging between 0.1 µm and 30 µm using Equations (13) and (14) [20].

$$\langle \overline{f_a} \rangle = 0.016 - 0.0023 r^{0.545} \quad (13)$$

$$\sigma_a' = 1.8 + 0.136 r^{1.4} \quad (14)$$

where r is the particle radius in μm.

By assuming that the aerodynamic couple acting on the particle are distributed following a Gaussian distribution, the resuspension rate constant can be formulated as function of the adhesive force f_a at the removal point as given by Equation (15):

$$p(f_a) = \frac{n_\theta \exp\left(\frac{-(f_a - \langle F \rangle)^2}{2\langle f^2 \rangle}\right)}{\frac{1}{2}\left\{1 + \text{erf}\left(\frac{f_a - \langle F \rangle}{\sqrt{2\langle f^2 \rangle}}\right)\right\}} \quad (15)$$

where, $F(t)$ is the force derived from the aerodynamic couples acting on the particle, $\langle F \rangle$, and f are the mean and the fluctuating parts of $F(t)$, erf is the Gauss error function, and n_θ is the value of the typical frequency of the forcing motion without resonance, given by Equation (16) [28]:

$$n_\theta \approx 0.00658\left(\frac{u^{*2}}{\nu}\right) \quad (16)$$

where u^* is the friction velocity (m.s^{-1}).

$$F(t) = \frac{1}{2}F_L + \frac{r}{a}F_D \quad (17)$$

where a is typical of the distance between asperities and $\frac{r}{a}$ is the geometric factor (the ratio of the particle radius to the distance between asperities of the surface roughness). According to Ref. [21] the geometric factor is assumed to be equal to 100. The drag and lift forces have been estimated using semi-empirical formula given by Equation (18) and (19) [28].

$$\frac{\langle F_L \rangle}{\rho \nu^2} \approx 20.9 (r^+)^{2.31} \quad (18)$$

$$\frac{\langle F_D \rangle}{\rho \nu^2} \approx 32 (r^+)^2 \quad (19)$$

where $r^+$is the dimensionless particle radius.

$$r^+ = \frac{r u^*}{\nu} \quad (20)$$

where r is the particle radius (m).

By injecting Equations (18) and (19) into Equation (17), we get the equation giving the variation of the mean force:

$$\frac{\langle F \rangle}{\rho \nu^2} = 10.45[1 + 300(r^+)^{-0.31}](r^+)^{2.31} \quad (21)$$

Ref. [28] measurements show that for a spherical particle in a turbulent boundary layer in an aerodynamically smooth channel, the ratio of the root mean square to the mean of lift force is approximately 0.2 (Equation (22)) and this ratio its roughly independent of the surface roughness.

$$\frac{\langle f^2 \rangle}{\langle F \rangle} = 0.2 \quad (22)$$

There is no available data on the ratio of the root mean square to mean of the drag force, so the value of this ratio is assumed to be equal to the that of the lift force.

Resuspension rates for variable shear velocity

The resuspension model in this study (Equation (9)) is suitable for a constant friction velocity. However, the transient nature of the flow in our study, implies a variable friction velocity. In this case, the simulation timestep (Δt) must be chosen small enough for considering a constant friction velocity during each time step. Thus, the resuspension rate will be averaged over a timestep Δt as given by Equation (23) (Ref. [18]).

$$\bar{\Lambda}(t) = \frac{1}{\Delta t}\int_0^{\Delta t} \Lambda(t)dt = \frac{1}{\Delta t}\int_0^{\infty} \varphi(\bar{f_a})(1 - e^{-p(\bar{f_a})\Delta t})d\bar{f_a} \qquad (23)$$

Equation (23) can be solved numerically with the following input parameters:

- **The size of the particles (particle diameter d_p)**: six sizes in the range 0.1 µm - 1 µm (d_p= 0.1 µm, 0.193 µm, 0.323 µm, 0.530 µm, 0.737 µm, 1 µm) were chosen for this study. These sizes were chosen in order to compare our numerical results to those of Ref. [7].
- **The particle and surface types**: this parameter is characterized by the thermodynamic work of adhesion (surface energy W_a) of the particle-substrate combination. The combinations used in this work are presented in Table 2. The reason for choosing these combinations was that linoleum is one of the most common building floorings. The second surface was selected to show the influence of the particle-surface characteristics, particularly the thermodynamic work of adhesion, on particle resuspension. Indeed, the thermodynamic work of adhesion of alumina-steel is about 28 and 65 times greater than that of PSL-linoleum and ATD-linoleum combinations respectively.

Table 2: Material properties of particle-substrate combinations that have been used in this study.

Particle	Substrate	W_a(J/m^2)	References
ATD (Arizona Test Dust)	Linoleum	8.56×10^{-3}	[16]
PSL (Polystyrene Latex Spheres)	Linoleum	19.86×10^{-3}	[16,29]
Alumina	Steel	0.56	[21]

- **The friction velocity**: It can be calculated using the Equation (24).

$$u^* = \sqrt{\frac{\tau_\omega}{\rho}} = \sqrt{\frac{\mu \left.\frac{du}{dy}\right|_{y=0}}{\rho}} \qquad (24)$$

where τ_ω is the wall shear stress and du/dy is the velocity gradient at the boundary.

- **The time step**.

In order to choose a time step adapted to our simulations it is necessary to examine the influence of this parameter on the average resuspension rate. Figure 4(a-b) presents an illustration of the variation of the average resuspension rate as a function of the time step for the three particle-substrate combinations and six particle sizes with friction velocities equal to 3 m/s. Note that for all cases, the variation of the average resuspension rate is less than 3 % for a certain critical time step Δt^*. The latter depends on the particle size and the particle-surface combination. For time steps higher than Δt^*, the resuspension rate decreases with the time step. Therefore, choosing a time step Δt greater than Δt^* leads to an underestimation of the resuspension rate.

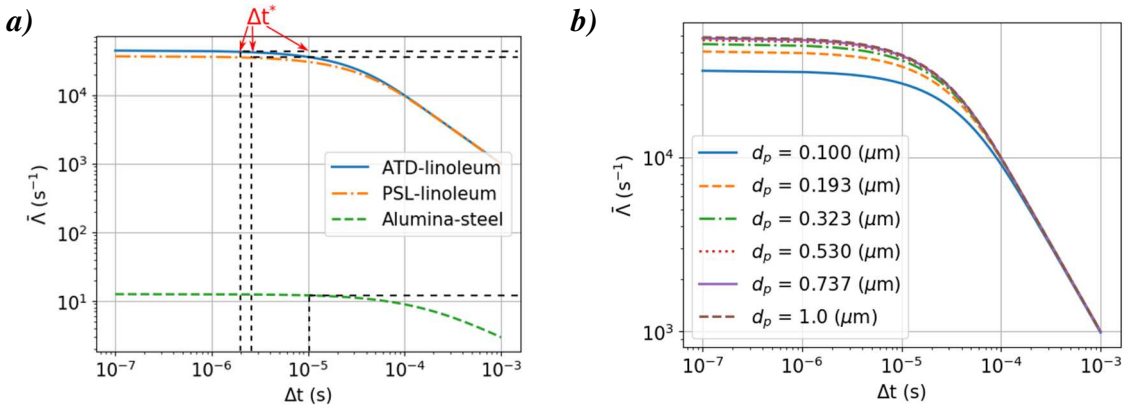

Figure 4. Average resuspension rate evolution as a function of the time step for u^*=3 m/s, a) for three different particle-substrate combinations with d_p= 0.323 μm, b) for six different diameters with ATD-linoleum.

Figure 5 represents the critical time step variation as a function of friction velocity for six different studied diameters and the three chosen combinations. First, it can be seen that Δt^* decreases sharply with the friction velocity. The influence of the particle size on Δt^* is negligible for the ATD-linoleum and PSL-linoleum combinations. On the other hand, if the particle size decreases, Δt^* decreases in the case of the alumina-steel combination. It can also be noted that Δt^* is not defined for friction velocities lower than a certain value, which depends on the particle size. This can be explained by the fact that, for low velocities, particles will not resuspend.

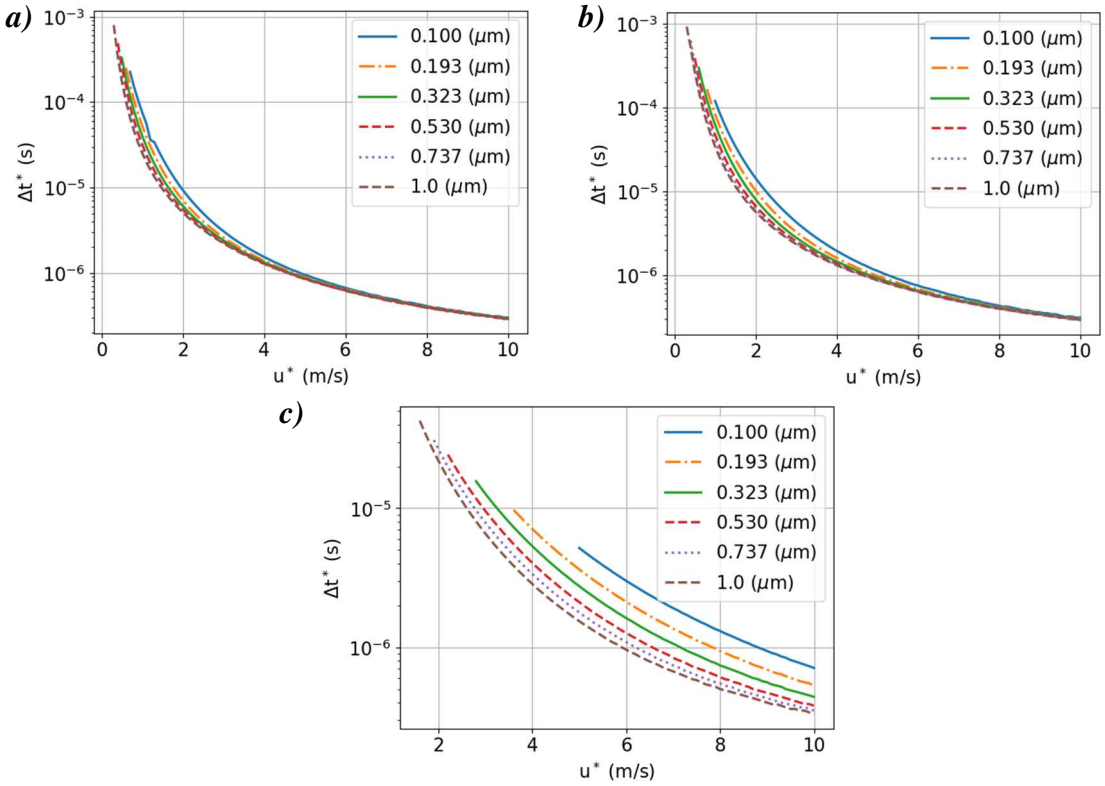

Figure 5. The critical time step Δt^* evolution as function of friction velocity for six different studied diameters, a) ATD-linoleum, b) PSL-linoleum, c) alumina-steel.

From this we can conclude that to avoid an underestimation of resuspension rates for all the studied cases, it is necessary to choose the time step that corresponding to the maximum friction velocity of all the simulations and the smallest particle size with the ATD-linoleum combination.

2.1.4 Grid independence study

Hybrid meshes were constructed with a fully structured hexahedral mesh in the domain, and a tetrahedral mesh in the shoe (see Figure 6). The wall y+ values near the ground were below 1, enabling appropriate resolution of the boundary layers.

A grid independence study was conducted in order to achieve accurate results while keeping the computation time within reason. Two parameters have been modified to create the three tested meshes (Table 3):

- The maximum cell size in the domain
- The maximum cell size in the shoe.

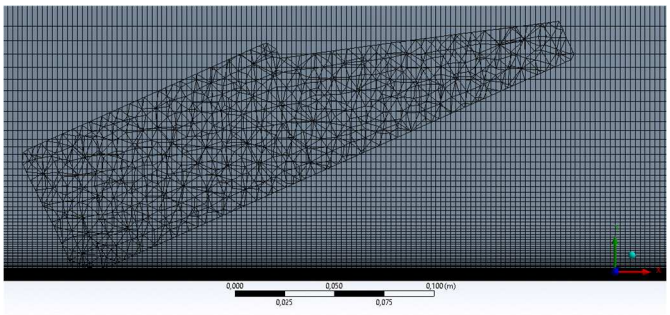

Figure 6. Grid configuration of the computational domain.

Table 3: Parameters of the three tested meshes.

Mesh	Coarse (M1)	Medium (M2)	Fine (M3)
Number of elements	1164617	3086494	8643107
The maximum cell size in the domain (m)	0.004	0.0025	0.0015
The maximum cell size in the shoe (m)	0.009	0.009	0.001

Figure 7 indicates the variation of the flow velocity below the shoe as a function of the height y at x=29.5 cm (see Figure 7(a)) for the three tested meshes. Accordingly, results with fine (M3) and medium (M2) mesh are very close, where the maximum percentage error is about 2 %, indicating that further refinement would not bring a significant additional accuracy that would outweigh the computational cost of enhancement. Thus, the second mesh (M2) is chosen for the remainder of this work.

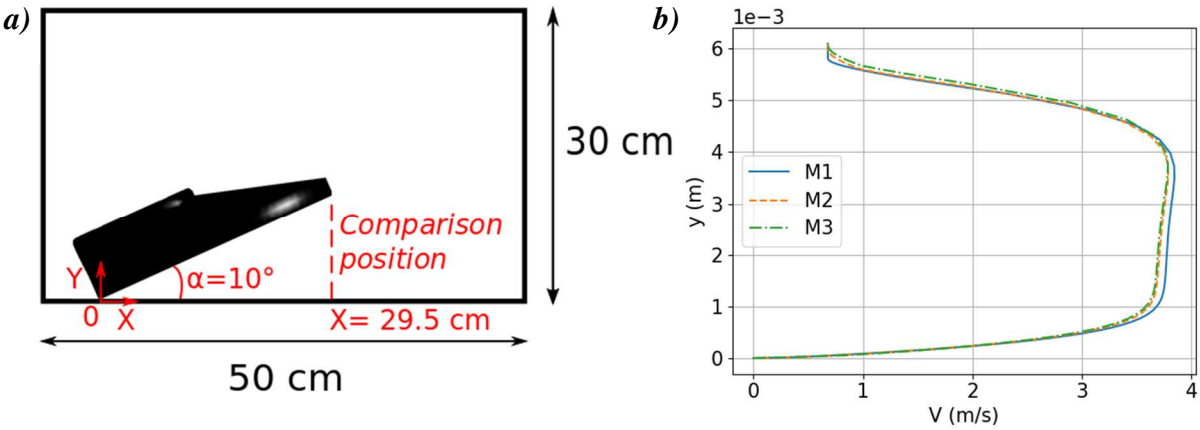

Figure 7. a) Comparison position, b) Variation of the flow velocity below the shoe as a function of the height y (at the end of the shoe) for the three studied meshes,

2.2 Shoe angular velocity measurement

One of the most important input parameters that influences particle resuspension is the shoe angular velocity [14, 10, 30]. To provide realistic angular velocities to our simulations, experiments were conducted using a FASTCAM SA5-1000K-M2 fast camera and a participant. The later, walked with three different speeds: slow walk, normal walk and fast walk. For each walking speed, the experiment was repeated ten times to ensure repeatability. The post-processing of the camera recordings using a MATLAB code gave the variation of the angle between the foot and the floor over time (see Figure 8). The foot speed was then estimated from the

average of the measurements from the different tests. The angular velocity equations are deduced by fitting the measured data with a 2nd-order polynomial equation.

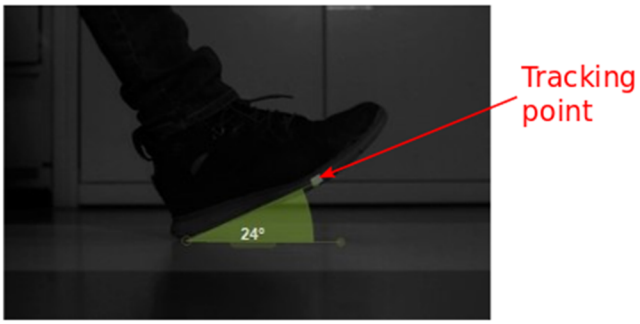

Figure 8. The position of the participant foot at the downward movement starting time.

Figure 9 shows the variation in the average angular velocity for the three different studied walking speed. Accordingly, for the different cases the angular velocity increases until reaching a maximum value of 210 °/s, 290 °/s, and 480 °/s for slow, normal, and fast walking, respectively. After that, the angular velocity decreases until the foot touches the ground with a velocity of 15 °/s, 100 °/s, and 180 °/s for slow, normal, and fast walking, respectively.

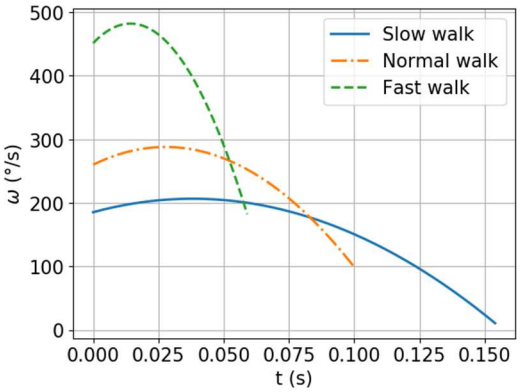

Figure 9. Variation of angular velocity of the foot for the three walking speeds.

2.3 Groove pattern

To investigate the impact of shoe grooves on particle resuspension, three types of shoes with different grooves were used (Figure 10): (1) shoe with no grooves, (2) shoe with 27 transverse grooves and (3) shoe with 13 longitudinal grooves. The width and depth of the grooves are 0.3 cm and 0.2 cm, respectively, for both the transverse and longitudinal cases. The distance between the grooves is 1 cm for both cases. The total areas for the shoes were the same at 220.72 cm^2. The contact area for shoes with grooves was 154.74 cm^2 for longitudinal, 154.45 cm^2 for transverse, and 220.72 cm^2 for shoes without grooves.

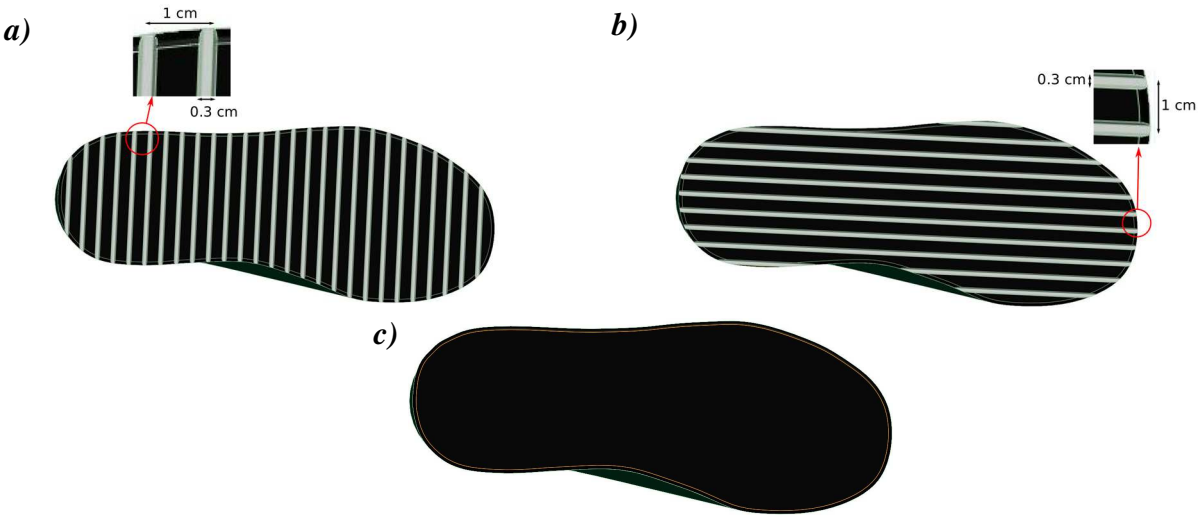

Figure 10. Descriptions for transverse (a), longitudinal (b) and no groove shoes (c) used for study.

3. Results and discussion

3.1 Airflow patterns

Figure 11(a) and Figure 11(b) show the velocity field generated by the human foot tapping motion in the case of a normal walk for shoe with no grooves for different instants along the longitudinal and lateral cross-sections, respectively. The figures are shown in sequence referenced at the time the shoe starts rotating. As shown in Figures 11(a1) and 11(b1), a tip vortex is developed at the edge of the shoe. Additionally, the flow under the shoe is squeezed and ejected as a wall jet in front of and from both sides of the shoe. This later leads to a high velocity region (10.17 m/s) near the wall (Figures 11(a2) and 11(b2)). By comparing the velocity in the two sections, we can see that the velocity generated in the lateral cross-section was higher than that generated at the longitudinal section (Figures 11(a2) and 11(b2)). After the shoe touches the floor, we note the formation of two counterrotating vortices translating horizontally on the ground and decaying slowly (Figures 11(a3) and 11(b3)). This phenomenon was also observed experimentally in Ref. [31].

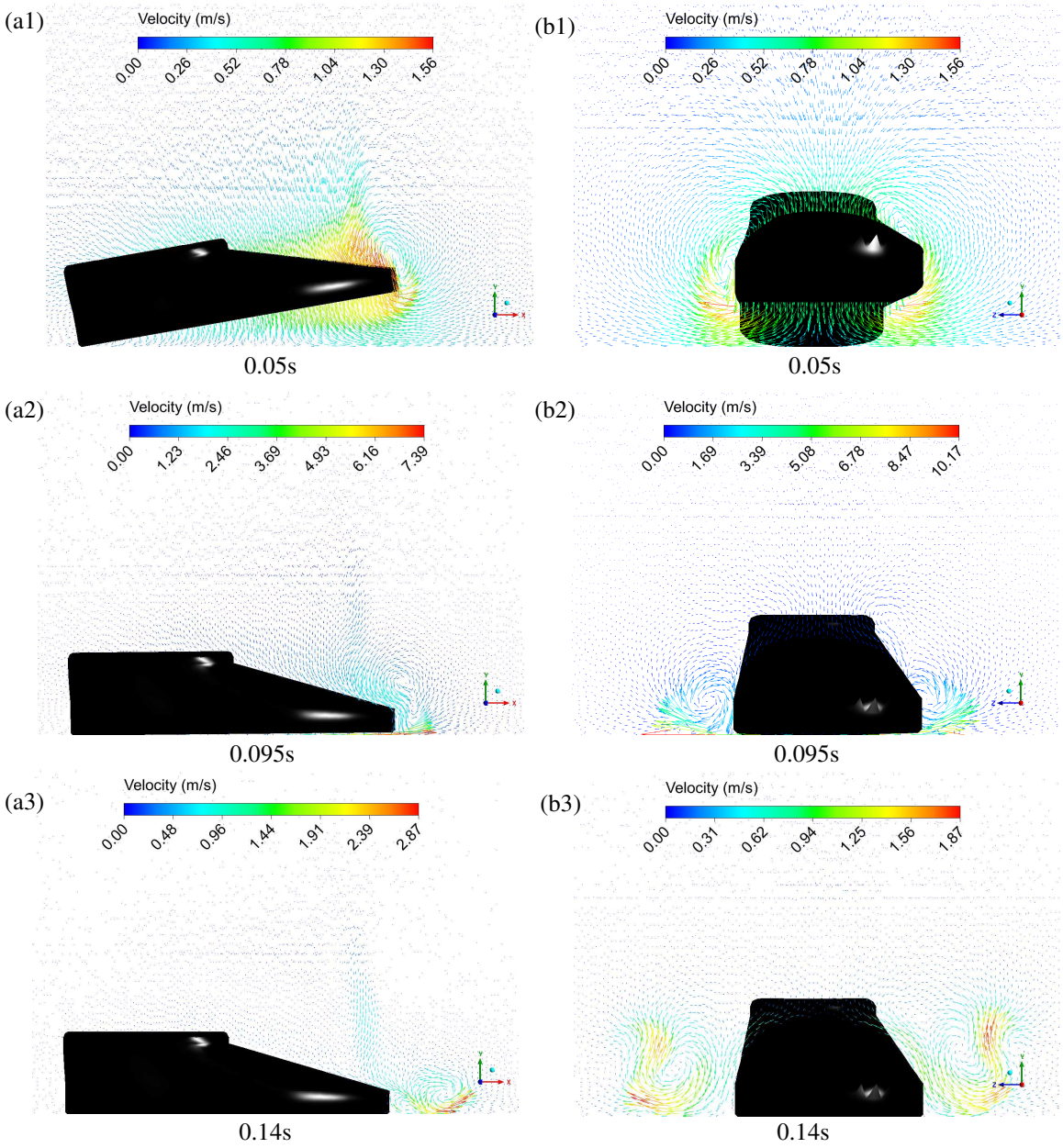

Figure 11. Velocity fields generated along the longitudinal (a1-a3) and transversal (b1-b3) sections.

As previously discussed, the friction velocity on the ground is one of the most important input parameters of the Rock 'n' Roll model that influence particle resuspension. Figure 12 shows the friction velocity fields on the ground at four different instants in the case of the normal walk. Accordingly, areas of high friction velocities are observed towards the heel, on the both sides and in front of the foot at 0.05 s, 0.095 s, 0.099 s respectively. These areas are the location of high velocity gradients generated by the jet of air ejected from the area under the foot. When the foot touches the ground (instant 0.1 s), the air underneath the foot is completely expelled to the outside creating a zone of high friction velocity in front of the foot. We notice that the maximum friction velocity increases as the shoe approaches the ground.

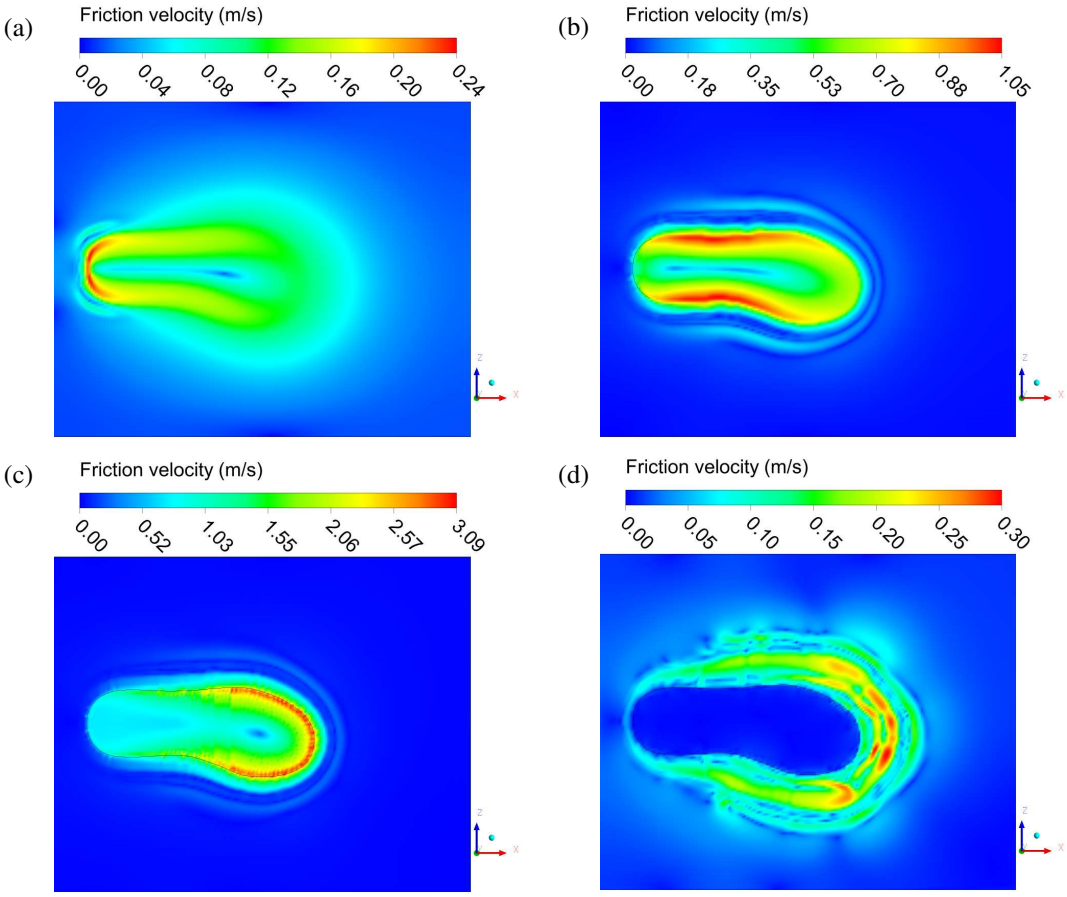

Figure 12. Friction velocity fields on the ground in four different times (referenced at the time the shoe starts rotating), a) t = 0.05 s, b) t = 0.095 s, c) t = 0.099 s, d) t = 0.14 s.

Before carrying out the multiphase simulations, it is essential to define a suitable time step. As previously discussed, the latter is conditioned by the maximum friction velocity (see Section 2.1.3). Figure 13 represent the maximum friction velocity variation as a function of time for different walking speed. 0 s is the instant at which the footstep starts rotation. For the three cases, the maximum friction velocity increases slowly and then sharply to reach 1.5 m/s, 4.4 m/s and 5.4 m/s in slow, normal, and fast walking cases, respectively. These values were reached at different times, which increased with the walking speed.

In view of these results, a time step of 1.25×10^{-6} s was chosen for our multiphase simulations, which corresponds to a friction velocity value of 5.4 m/s (fast walk). This time step guarantees a constant average resuspension rate (Figure 5, Section *2.1.3*) for the three cases.

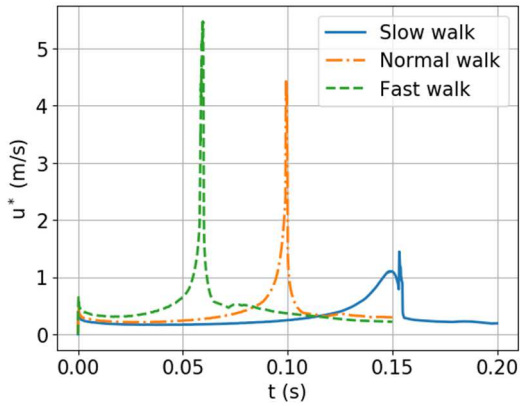

Figure 13. Variation of maximum friction velocity on the ground for three walking speed.

3.2 Comparison with previous experimental study

Figure 14 represents the resuspended particle mass flow rate of the particles versus time for the studied particle sizes during and after the footstep in the case of a normal walk and the ATD-linoleum combination. 0 s is the instant at which the footstep starts rotation. The figure shows that the resuspended particle mass flow rate evolutions for the different particle sizes have the same shape. First, no particles are resuspended between 0 s and 0.095 s and between 0.103 s and the end of the simulation. This can be explained by the fact that the particle has not accumulated enough vibrational energy from the turbulent flow to be detached itself from the surface. Second, between 0.095 s and 0.103 s, the particle mass flow rate of the different sizes increased sharply until reaching different levels, depending on the particle size. This finding is consistent with prior studies, which found that human walking significantly increases particle concentrations of different sizes in indoor environments. Comparing the results of different sizes, it can be determined that the highest resuspended particle mass flow rate was approximately 5×10^{-5} kg/s for 0.530 µm particles.

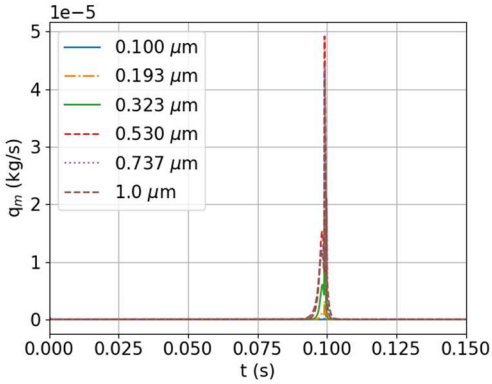

Figure 14. Typical resuspended particle mass flow rate profile for a representative simulation.

Figure 15 shows the variation of the resuspended fraction as a function of particle size in the ATD-linoleum case with a normal walking speed compared with the experimental data of Ref. [7]. It can be seen that resuspension fractions range over two orders of magnitude from 10^{-4} to 10^{-2}. It can be noted that there is a good agreement between the numerical and experimental particle resuspended fraction profiles with a slight difference. This difference is probably due to the error in the walking speed measurement or not taken into account the shoe flexibility. In addition, in the case of the experimental measurements, the resuspension fraction is calculated for an average of 48 steps/min during a time of 10 min, while in the numerical simulations it is calculated for a single step. Indeed, particle resuspension fractions increased with the particle size. This is probably due to particle adhesion forces, such as electrostatic forces, which increase as the particle size decreases and tend to keep particles attached to the ground surface [32, 33].

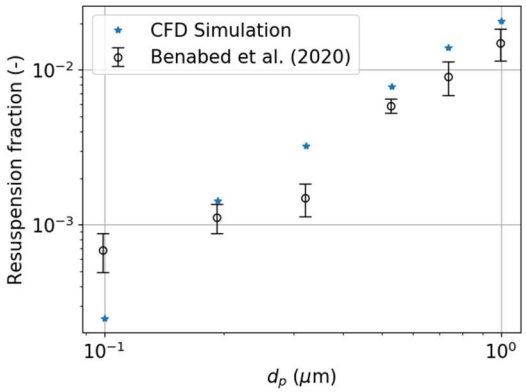

Figure 15. Comparison of the resuspension fraction with Ref. [7].

3.3 Groove patterns influence

Figure 16 shows the variation in the resuspended fraction as a function of particle size for the three types of groove patterns (no groove, longitudinal and transversal grooves) with the ATD-linoleum combination. Note that for particles sizes greater than 0.193 µm no significant difference between the shoe groove patterns was observed, which corresponds with the Ref. [13] experimental results (for sizes greater than 0.8 µm). For particle sizes less than 0.193 µm, the fraction is slightly higher for shoes with longitudinal grooves than for shoes without grooves and transverse grooves.

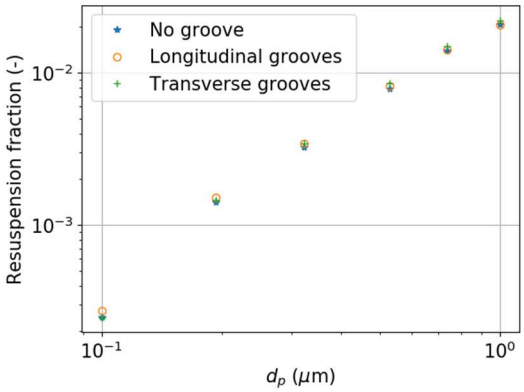

Figure 16. Resuspension fractions associated with shoes of various groove patterns for six particle sizes for the ATD-linoleum combination.

3.4 Walking speed and particle-substrate combination influence

The simulation results show that, regardless of the walking speed and particle size, no resuspension occurred in the alumina-steel combination. Figure 17 shows the variation of the resuspended fraction with particle size for three different walking speeds and different particle-substrate combinations. Accordingly, the resuspension fraction increases with walking speed for the different particle sizes, with about an order of magnitude between fast and normal walking and between normal and slow walking. For the latter, no resuspension was occurred for particles smaller than 0.193 µm and 0.323 µm in the ATD-linoleum and PSL-linoleum cases, respectively. In addition, the resuspension fraction for all particle sizes is larger for the ATD-linoleum combination (with a maximum of 0.9 in the fast walk case) than for the PSL-linoleum combination. This can be explained by the difference between the thermodynamic work of adhesion of the particle-substrate considered combination.

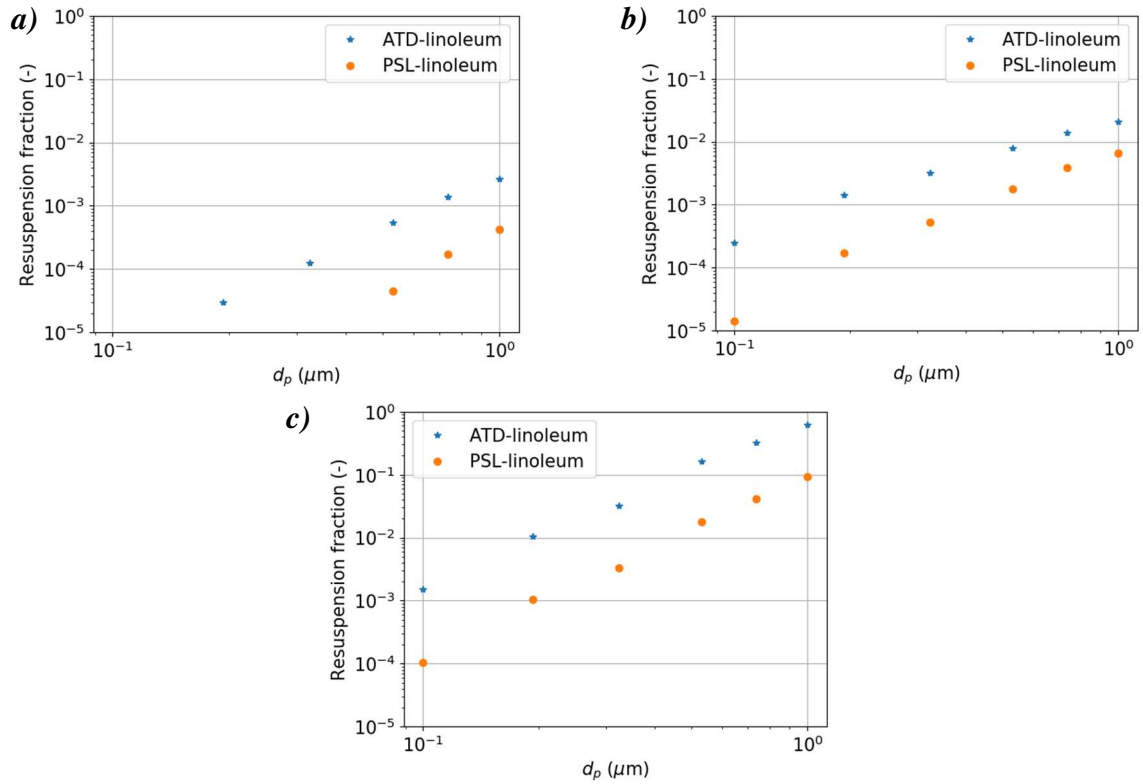

Figure 17. Comparison of the resuspension fraction for two different selected particle-substrate combinations, a) Slow walk, b) Normal walk, c) Fast walk

4. Conclusion

In this work, unsteady numerical simulations using ANSYS CFX software were conducted to study the airflow and resuspension of particles smaller than 1 µm (≤1 µm) generated by human foot tapping motion during the walking process. The immersed solid method was used to incorporate the shoe in a three-dimensional geometry. The particle resuspension fraction was estimated using the Rock 'n' Roll model was used to predict. Three sole patterns (no groove, transverse and longitudinal) were investigated, and three different selected particle-substrate combinations (ATD-linoleum, PSL-linoleum and alumina-steel) were tested. Three profiles of human footstep speed variations during walking were obtained by analyzing a real human walk. These profiles were used as inputs for the numerical simulations.

Simulations showed the formation of a flow jet due to the expulsion of the air under the shoe. After the shoe touched the ground, vortices were formed beside and in front of the shoe. During the shoe rotation, areas of high friction Velocities were observed towards the heel, on both sides, and in front of the foot.

The particle resuspension result of this work was compared with the experimental data from the literature, and a good agreement was found. This work reveals some important information regarding particle resuspension in indoor environments. The simulations show that human step resuspended particles of sizes ranging from 0.1 to 1 µm under certain conditions. The resuspension fraction ranges over four orders of magnitude, from 10^{-5} to 10^{-1}. Particle and surface types largely influence resuspension. Indeed, in the case of the combination alumina-steel, the step did not resuspend any particles. Also, it was confirmed that high stepping velocity increases particle resuspension. This influence may explain the large discrepancy between some previous experimental studies. Finally, result show that shoe patterns have no significant influence on particle resuspension.

The present work has refined the level of knowledge on the phenomenon of resuspension by human walking. Additional studies are needed to understand the resuspension for particles smaller than 0.1 µm and the impact of other parameters such as shoe material and flexibility.

Acknowledgments

The agglomeration committee of La Rochelle CDA and the Mechanic Laboratory of the Royal Military Academy in Brussels are gratefully acknowledged.

References

[1] Sacks JD, Stanek LW, Luben TJ, et al. Particulate Matter–Induced Health Effects: Who Is Susceptible? *Environ Health Perspect*. 2011;119(4):446-454. doi:10.1289/ehp.1002255

[2] Peters A, Wichmann HE, Tuch T, Heinrich J, Heyder J. Respiratory effects are associated with the number of ultrafine particles. *Am J Respir Crit Care Med*. 1997;155(4):1376-1383. doi:10.1164/ajrccm.155.4.9105082

[3] Ferro AR, Kopperud RJ, Hildemann LM. Source Strengths for Indoor Human Activities that Resuspend Particulate Matter. *Environ Sci Technol*. 2004;38(6):1759-1764. doi:10.1021/es0263893

[4] Thatcher T. Deposition, resuspension, and penetration of particles within a residence. *Atmos Environ*. 1995;29(13):1487-1497. doi:10.1016/1352-2310(95)00016-R

[5] Tian Y, Sul K, Qian J, Mondal S, Ferro AR. A comparative study of walking-induced dust resuspension using a consistent test mechanism. *Indoor Air*. 2014;24(6):592-603. doi:10.1111/ina.12107

[6] Benabed A, Limam K, Janssens B, Bosschaerts W. Human foot tapping-induced particle resuspension in indoor environments: Flooring hardness effect. *Indoor Built Environ*. 2020;29(2):230-239. doi:10.1177/1420326X19856054

[7] Benabed A, Boulbair A, Limam K. Experimental study of the human walking-induced fine and ultrafine particle resuspension in a test chamber. *Build Environ*. 2020;171:106655. doi:10.1016/j.buildenv.2020.106655

[8] Henry C, Minier JP. Progress in particle resuspension from rough surfaces by turbulent flows. *Prog Energy Combust Sci*. 2014;45:1-53. doi:10.1016/j.pecs.2014.06.001

[9] Serfozo N, Chatoutsidou SE, Lazaridis M. The effect of particle resuspension during walking activity to PM 10 mass and number concentrations in an indoor microenvironment. *Build Environ*. 2014;82:180-189. doi:10.1016/j.buildenv.2014.08.017

[10] You S, Wan MP. Experimental investigation and modelling of human-walking-induced particle resuspension. *Indoor Built Environ*. 2015;24(4):564-576. doi:10.1177/1420326X14526424

[11] Rosati JA, Thornburg J, Rodes C. Resuspension of Particulate Matter from Carpet Due to Human Activity. *Aerosol Sci Technol*. 2008;42(6):472-482. doi:10.1080/02786820802187069

[12] Zhang X, Ahmadi G, Qian J, Ferro A. Particle Detachment, Resuspension and Transport Due to Human Walking in Indoor Environments. *J Adhes Sci Technol*. 2008;22(5-6):591-621. doi:10.1163/156856108X305624

[13] Lai ACK, Tian Y, Tsoi JYL, Ferro AR. Experimental study of the effect of shoes on particle resuspension from indoor flooring materials. *Build Environ*. 2017;118:251-258. doi:10.1016/j.buildenv.2017.02.024

[14] Qian J, Ferro AR. Resuspension of Dust Particles in a Chamber and Associated Environmental Factors. *Aerosol Sci Technol*. 2008;42(7):566-578. doi:10.1080/02786820802220274

[15] Qian J, Ferro AR, Fowler KR. Estimating the Resuspension Rate and Residence Time of Indoor Particles. *J Air Waste Manag Assoc*. 2008;58(4):502-516. doi:10.3155/1047-3289.58.4.502

[16] Goldasteh I, Ahmadi G, Ferro AR. Wind tunnel study and numerical simulation of dust particle resuspension from indoor surfaces in turbulent flows. *J Adhes Sci Technol*. 2013;27(14):1563-1579. doi:10.1080/01694243.2012.747729

[17] Oberoi RC, Choi JI, Edwards JR, Rosati JA, Thornburg J, Rodes CE. Human-Induced Particle Re-Suspension in a Room. *Aerosol Sci Technol*. 2010;44(3):216-229. doi:10.1080/02786820903530852

[18] Choi JI, Edwards JR, Rosati JA, Eisner AD. Large Eddy Simulation of Particle Re-suspension During a Footstep. *Aerosol Sci Technol*. 2012;46(7):767-780. doi:10.1080/02786826.2011.631613

[19] Reeks MW, Reed J, Hall D. On the resuspension of small particles by a turbulent flow. *J Phys Appl Phys*. 1988;21(4):574-589. doi:10.1088/0022-3727/21/4/006

[20] Biasi L, de los Reyes A, Reeks MW, de Santi GF. Use of a simple model for the interpretation of experimental data on particle resuspension in turbulent flows. *J Aerosol Sci*. 2001;32(10):1175-1200. doi:10.1016/S0021-8502(01)00048-9

[21] Reeks MW, Hall D. Kinetic models for particle resuspension in turbulent flows: theory and measurement. *J Aerosol Sci*. 2001;32(1):1-31. doi:10.1016/S0021-8502(00)00063-X

[22] Goldasteh I, Tian Y, Ahmadi G, R. Ferro A. Human induced flow field and resultant particle resuspension and transport during gait cycle. *Build Environ*. 2014;77:101-109. doi:10.1016/j.buildenv.2014.03.016

[23] Goldasteh I, Ahmadi G, Ferro A. A Model for Removal of Compact, Rough, Irregularly Shaped Particles from Surfaces in Turbulent Flows. *J Adhes*. 2012;88(9):766-786. doi:10.1080/00218464.2012.694278

[24] Gélain T, Rondeau A, Peillon S, Sabroux JC, Gensdarmes F. CFD modelling of the wall friction velocity field in the ITER tokamak resulting from airflow during a loss of vacuum accident—Consequences for particle resuspension. *Fusion Eng Des*. 2015;100:87-99. doi:10.1016/j.fusengdes.2015.04.043

[25] Yoon Y, Park BH, Shim J, Han YO, Hong BJ, Yun SH. Numerical simulation of three-dimensional external gear pump using immersed solid method. *Appl Therm Eng*. 2017;118:539-550. doi:10.1016/j.applthermaleng.2017.03.014

[26] ANSYS User's Manual.

[27] Gelain T, Gensdarmes F, Peillon S, Ricciardi L. CFD modelling of particle resuspension in a toroidal geometry resulting from airflows during a loss of vacuum accident (LOVA). *Fusion Eng Des*. 2020;151:111386. doi:10.1016/j.fusengdes.2019.111386

[28] Hall D. Measurements of the mean force on a particle near a boundary in turbulent flow. *J Fluid Mech*. 1988;187:451-466. doi:10.1017/S0022112088000515

[29] Phares DJ, Smedley GT, Flagan RC. EFFECT OF PARTICLE SIZE AND MATERIAL PROPERTIES ON AERODYNAMIC RESUSPENSION FROM SURFACES. *J Aerosol Sci*. 2000;31(11):1335-1353. doi:10.1016/S0021-8502(00)00034-3

[30] Mana Z. Étude sur la remise en suspension de particules suite à la marche d'un opérateur. Published online 2014.

[31] Benabed A, Limam K, Janssens B, Bosschaerts W, Vercauteren J. Experimental investigation of the flow field generated by idealized human foot tapping. *Sci Technol Built Environ*. 2020;26(2):229-236. doi:10.1080/23744731.2019.1614427

[32] Feng JQ, Hays DA. Relative importance of electrostatic forces on powder particles. *Powder Technol*. 2003;135-136:65-75. doi:10.1016/j.powtec.2003.08.005

[33] Walton OR. Review of Adhesion Fundamentals for Micron-Scale Particles. *KONA Powder Part J*. 2008;26(0):129-141. doi:10.14356/kona.2008012